Korean J. Chem. Eng., 33(5), 1647-1652 (2016)
DOI: 10.1007/s11814-016-0008-7

pISSN: 0256-1115
eISSN: 1975-7220

Effects of surfactants on the preparation of TiO_2 nanoparticles in microwave-assisted sol-gel process and their photocatalytic activity

Inseok Jang, Hui Jun Leong, and Seong-Geun Oh†

Department of Chemical Engineering, Hanyang University, Seoul 04763, Korea
(*Received 3 October 2015 • accepted 7 January 2016*)

Abstract−Nanosized TiO_2 particles were prepared through facile sol-gel reaction by using microwave-assisted method. To investigate the effects of surfactants on the formation of TiO_2, various additives (PVP, Triton X-100 and P123) were employed. The diameter of synthesized titania spheres could be controlled from 105 to 380 nm. The TiO_2 particles prepared with P123 triblock copolymer showed large surface area and high pore volume. It was attributed to the fact that the pore site, where the surfactant template initially existed, was generated upon calcination process. The characteristics of prepared TiO_2 nanoparticles were analyzed by using FE-SEM, TEM, XRD, FT-IR and N_2 adsorption-desorption. As an application of prepared composites for water treatment, their photocatalytic performances for the degradation of methylene blue dye were examined by using UV-vis spectrophotometer under room light irradiation. The prepared TiO_2 particles with Triton X-100 and P123 exhibited higher performance for methylene blue photo-degradation than that of P25. It was attributed to the effects of large specific surface area and high porosity.

Keywords: Surfactant, TiO_2, Surface Area, Photocatalytic Activity

INTRODUCTION

Over the past few decades, photocatalytic degradation of harmful organic pollutants in the air and water using semiconductor catalysts has attracted extensive attention [1,2]. Among the numerous semiconductors, titanium dioxide (TiO_2) particles have been widely used in various environmental purification applications such as antibacterial treatment, self-cleaning and deodorization as well as the photo-decomposition of organic pollutant in aqueous solution owing to its outstanding characteristics including a high physical and chemical stability, nontoxic property for human body and low cost [3]. In 1972, Fujishima and Honda discovered the phenomenon of photocatalytic splitting of water molecule under ultraviolet (UV) light into hydrogen and oxygen on TiO_2 electrode which has a bandgap of 3.0-3.2 eV. It was the beginning of a new era in heterogeneous photocatalysis [4]. Hitherto, various attempts had been made to enhance the photo-electrochemical activity of TiO_2. For instance, the immobilization of metal (e.g., Pt, Au, Ag, and so on) on the TiO_2 surface can form a Schottky barrier and this energy barrier serves as an efficient electron trapping sites preventing electron-hole recombination in photocatalysis [5-8]. In case of the nonmetal-TiO_2 composites such as N-, C-, F- and S-TiO_2, an effective approach to drive the absorption of TiO_2 in visible light region has been proven [9-12]. Consequently, high photocatalytic activity can be achieved by band edge shift. Among many technical approaches to enhance the photocatalytic activity, the studies for nano-scale particles have attracted an increasing attention due to the excellent advantages related to their small size (e.g., large surface area, high activity, high colloidal dispersion stability, etc.) [13-16]. Despite these advantages, there are several problems for usage of TiO_2. First, it is very difficult to handle nanoparticles, because they are governed not by both gravity and centrifugal force but by van der Waals force and electrostatic force [17]. It causes difficulties of separation and recovery of catalyst. Also, their small size tends to agglomerate into large particles to reduce their surface energy, resulting in the reduction of catalyst performance. Consequently, these disadvantages of nanosized particles lead to high costs. For these reasons, many researchers have focused on mesoporous TiO_2 materials because they do not only take advantage of high surface area but also make the catalyst-recovering stage less troublesome [18,19]. Tompsett et al. have reviewed the microwave synthesis of nanoporous materials. They proposed that the time for the synthesis of nanoporous materials can be dramatically decreased and the distributions of crystallite/particle dimensions can be significantly narrow. Several studies have suggested this implies more rapid nucleation of the initial crystallites, while others suggest that the growth process is more uniform [20].

In the present study, mesoporous structured TiO_2 nanoparticles were synthesized by using facile microwave-assisted sol-gel method. We focused on the investigation of the effect of surfactants on the formation of TiO_2 nanoparticles. To enhance the catalytic activity in aqueous solution, hydroxyl groups were introduced onto the surface of prepared TiO_2 powder by using hydroxylation treatment. Methylene blue decomposition was used as probe reactant to evaluate the photocatalytic activity of prepared TiO_2 nanoparticles under room light irradiation. Compared to commercial P25, higher photocatalytic activities were exhibited in TiO_2 prepared with TritonX-100 and P123. It is attributed to the larger surface area, higher porosity resulted from effect of surfactant on the formation of TiO_2 particles.

†To whom correspondence should be addressed.
E-mail: seongoh@hanyang.ac.kr

EXPERIMENTAL

1. Materials

Titanium(IV) isopropoxide (TTIP, 98.0%) as a precursor was obtained from Junsei in Japan. Isopropyl alcohol (IPA, 99.5%) was purchased from Daejung in Korea. Ammonia solution (NH_4OH, 25-27.9%) employed as a basic catalyst was purchased from Wako in Japan. Polyvinylpyrrolidone (PVP, Mw: ~55000), TritonX-100 (laboratory grade) and poly(ethylene glycol)-poly(propylene glycol)-poly(ethylene glycol) triblock copolymer (P123, Mn: 5800) purchased from Sigma-Aldrich were used to investigate the effect of surfactant on formation of TiO_2 particles. Methylene blue (MB, 97.0%) used as an organic pollutant and hydrogen peroxide solution (H_2O_2, 30.0%) were obtained from Daejung in Korea. The most popular commercial form of TiO_2 powder under the name of P25 (average diameter: 25 nm, containing phase: 80% of anatase and 20% of rutile) was obtained from Degussa. All chemical reagents used in experiments were analytical grades and used without any further purification. The water used in all experiments was double-distilled and deionized by the Milli-Q Plus system (Millipore, France) having 18.2 MΩ·cm electrical resistivity at 25 °C.

2. Facile Synthesis of TiO_2 Nanoparticles

For facile TiO_2 preparation, microwave-assisted sol-gel reaction process was performed. Mixed solution (IPA : H_2O=1 : 1 (w : w)) was pre-heated for 1 min by using microwave (700 W) and then 6.62 g of different additives (PVP, TritonX-100 and P123) and NH_4OH (0.66 g) was added into the solution under vigorous stirring at room temperature until the solution was completely dissolved. Subsequently, TTIP as a precursor was added drop by drop into the reaction medium under magnetic stirring. After 1 min, the suspension was heated by microwave for 1 min to finalize the reaction (Care had to be taken because there is a possibility of alcohol explosion attributed to microwave local heating). The resultant solution was washed with ethyl alcohol three times and dried at 50 °C. Finally, the obtained powder was calcined at 500 °C for 3 h to remove the residual organic reagents and to gain the crystal structure of TiO_2. The samples, which were prepared with different surfactants (PVP, Triton X-100 and P123), were identified as T-PVP, T-TX and T-P123, respectively. To compare the photocatalytic performance of prepared TiO_2 particles, the commercial P25 powder was employed as a reference.

3. Hydroxylation Treatment

To introduce hydroxyl groups on the TiO_2 surface, 0.5 g of the TiO_2 powder was added into aqueous NH_4OH solution (2 M) at 70 °C for 6 h in each sample. The resultants were rinsed with water and then dried at 50 °C for 12 h.

4. Photocatalytic Activities of the TiO_2 Particles

Photocatalytic performance of TiO_2 particles was estimated through the degradation of aqueous MB solution under a room light at 25 °C. In each sample, the 0.05 g of TiO_2 powder was dispersed in 100 mL of aqueous MB solution with a concentration of 1×10^{-5} M. Prior to irradiation, the suspension was magnetically stirred in dark for 30 min to allow the system to reach an adsorption/desorption equilibrium between catalyst and MB molecules. The suspension was kept constant under air-equilibrated conditions before and during irradiation. At given irradiation time intervals (20 min), 7.5 mL of suspension was extracted and centrifuged to separate the particles and then the MB concentration in the supernatant solution was determined by measuring the UV-Vis absorbance of aqueous dye solution at a wavelength of 665 nm.

5. Characterizations

The morphological property of synthesized TiO_2 particles was observed by field emission scanning electron microscope (FE-SEM, JEOL, JSM-6700F) and high resolution transmission electron microscope (TEM, JEOL, JEM-2100F). Before the analysis of FE-SEM, all samples were coated with platinum by sputtering at 15 mA for 3 min using a coating machine. To obtain specimens for TEM analysis, the particles were redispersed in ethanol. A drop of diluted solution was placed on the TEM grid and dried in drying oven at 70 °C for 1 day prior to observation. The X-ray diffractometer (XRD, Rigaku, D/MAX-2500) was operated to identify the crystal structure of TiO_2 particles. The incident wavelength was Cu Kα radiation (λ=1.54056 Å) and the detector moved step by step ($\Delta 2\theta$=0.05°) between 10 and 80° 2θ with 2°/min of scan speed. Fourier transform infrared spectrometer (FT-IR, Varian 640-IR) was employed to confirm the presence of organic template in the prepared sample. The specific surface area of product was measured by N_2 adsorption-desorption isotherm measurements at 77 K using Brunauer-Emmett-Teller surface area apparatus (BET, BELSORP-mini II). Pore volume and pore size were calculated by using Barrett-Joyner-Halenda (BJH) model on the desorption branch. The photocatalytic property of prepared TiO_2 particles was measured by UV-Vis spectrophotometer (Agilent Technologies, Agilent 8435).

RESULTS AND DISCUSSION

1. Synthesis Mechanism and Size Control

The spherical TiO_2 nanoparticles were synthesized with various surfactants via microwave assisted sol-gel method. For the investigation into the effect of surfactants on morphological property, experiments with different surfactants were performed. Fig. 1 shows the effect of surfactants on the formation of TiO_2 nanoparticles. In the case that the surfactant was absent, the shape of TiO_2 was irregular and their particle size distribution was broader as shown in Fig. 1(a). In sol-gel reaction, hydrolysis and condensation reactions took place when the alkoxide precursor reacted immediately in the presence of water leading to formation of larger and heterogeneous product [21]. On the other hand, the monodispersed TiO_2 spheres were observed in all other samples. As shown in Fig. 1(b), (c) and (d), the average diameters of T-PVP, T-TX, and T-P123 were 155, 105 and 380 nm as shown in SEM images. Their size is indicated in Table 1. There are differences in particles size because of the difference of surfactant behavior and micellar structures. Interestingly, prepared TiO_2 by using P123 surfactant were composed of very small particles with diameter of 20 nm as in the inset image of Fig. 1(d). It was expected that the growth step of primary particle was suppressed by P123 polymer triblock copolymer, which has a more complex structure compared to that of T-TX and T-PVP. Thus, smaller TiO_2 particles could be obtained by using P123 polymeric surfactant [22]. The plausible formation mechanism of TiO_2 nanoparticles could be proposed as illustrated in Fig. 2(a). (i) When the concentration of surfactant was above critical micelle concentra-

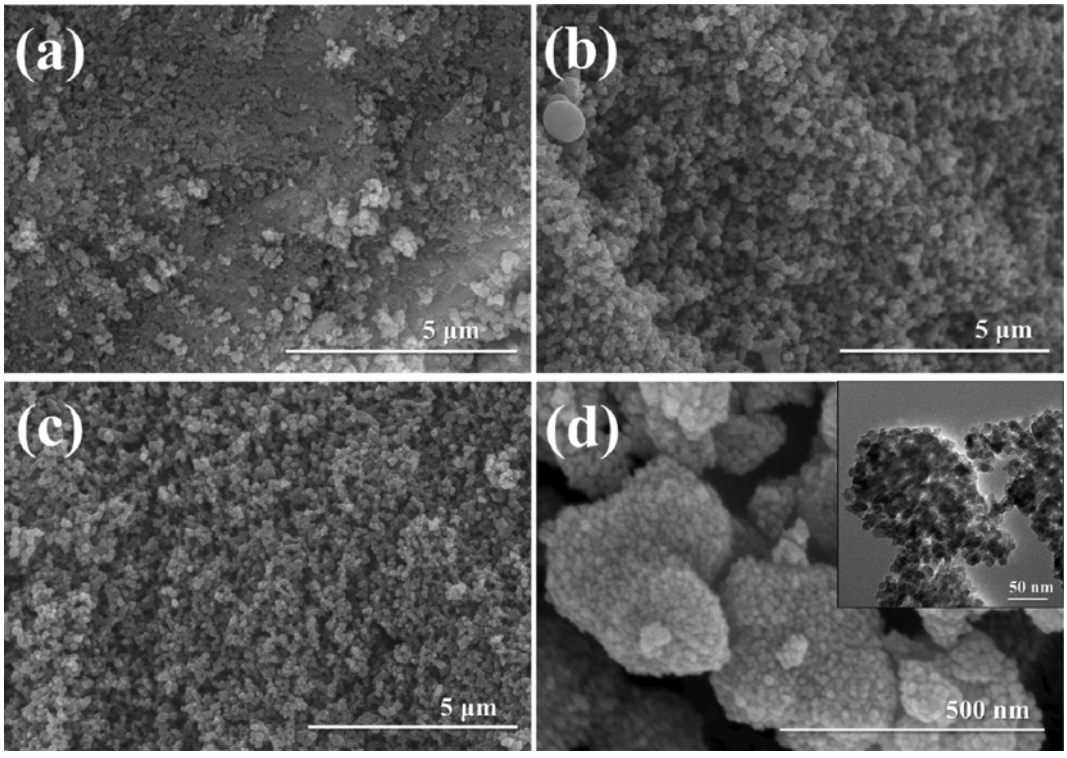

Fig. 1. FE-SEM images of prepared TiO_2 without surfactant (a), T-PVP (b), T-TX (c) and T-P123 (d) and inset image indicates TEM image.

Table 1. Estimations of particle size, crystal structure, BET surface area (S_{BET}), pore volume and average pore diameter of samples

Samples	Particle size (nm)	Crystal structure	S_{BET} (cm^2/g)	Pore volume (cm^3/g)	Average pore diameter (nm)
T-PVP	155	Anatase+Rutile	9.53	0.072	30.93
T-XT	105	Anatase	49.25	0.196	14.54
T-P123	380	Anatase	97.01	0.306	11.20
P25	25	Anatase+Rutile	56.92	0.118	10.66

tion (CMC), surfactant molecules formed micelles in aqueous solution to achieve a thermodynamically stable state. (ii) When TTIP precursor was added into the micellar solution, TiO_2-surfactant complex was formed by the interaction between hydrolyzed TTIP and hydrophilic part of surfactant based on the hydrogen bonding (Fig. 2(b)). Subsequently, further hydrolysis and condensation reactions proceeded and then, the growth step was carried out for the formation of TiO_2 nanoparticles. Finally, (iii) the mesoporous structured TiO_2 could be obtained after the removal of template through calcination process.

Fig. 3 indicates the FT-IR of prepared TiO_2 particles in the range from 700 to 4,000 cm^{-1}. The broad band at 3,400 cm^{-1} is ascribed to adsorbed H_2O molecules and surface -OH groups [23]. The strong band located at ~1,000 cm^{-1} was ascribed to T-O stretching and Ti-O-Ti bridge stretching modes [24]. In T-PVP curve, the weak band at 2,930 cm^{-1} s was attributed to the stretching vibration of C-H in PVP molecular structure and the peak at 1,651 cm^{-1} to the amide I band [25]. The T-PVP peaks at 1,095 and 1,039 cm^{-1} corresponded to Ti-OH stretching motions and Ti-OC_4H_9 bending, respectively [26]. The characteristic T-TX peaks at 1,637, 1,090 and 1,056 cm^{-1} were assigned as v_{c-c} of benzene, ϕ-O and C-O stretching vibrations, respectively [27]. In the curve of T-P123, the peak located at 2,933 cm^{-1} was ascribed to stretching vibration (-CH_3- and -CH_2-) and the peak at 1,456 cm^{-1} to bending vibration (C-H). From this result, the presence of organic materials such as PVP, Triton X-100 and P123, which interacted with TiO_2, could be confirmed. It indicated that surfactants acted as a template for the formation of nanoparticles.

2. Crystal Structure and Surface Area

Fig. 4 shows the XRD patterns of synthesized TiO_2 and P25 and their crystal phase is listed in Table 1. In the XRD pattern of T-PVP prepared without calcination process, the curve indicates amorphous crystal structure. On the other hand, after thermal treatment at 500 °C for 3 h, the main peaks of all samples were clearly observed at 2θ (25.30, 37.82 and 48.06°) and they were assigned as the (1 0 1), (0 0 4) and (2 0 0), respectively (JCPDS No. 21-1272). Interestingly, the diffraction pattern of calcined T-PVP displayed not only the anatase phase but also the peaks at 27.34, 35.96 and 41.10° of rutile phase (JCPDS No. 21-1276). The XRD results of T-PVP could be explained as follows. PVP played an important role in the crystallization of titania, because the distortion of the structure of TiO_2 was attributed to the organic groups of PVP

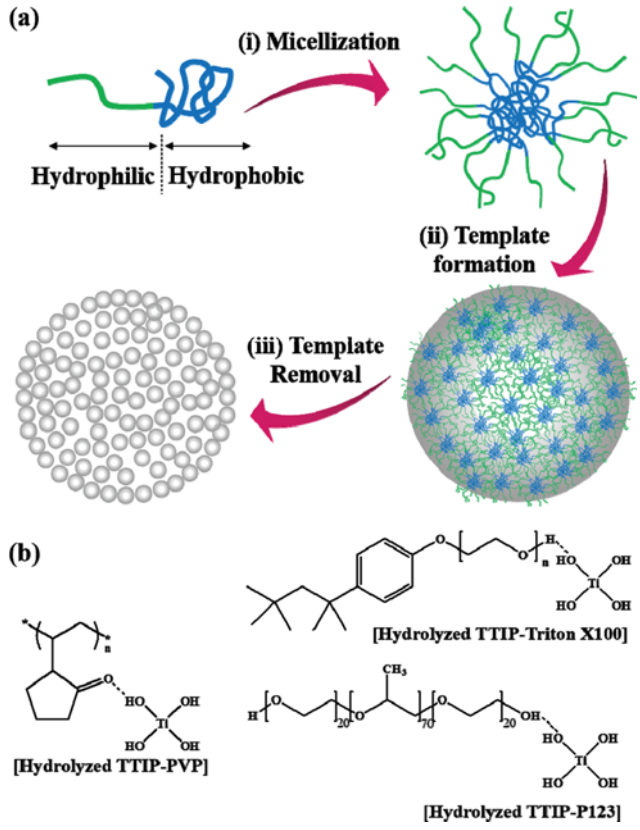

Fig. 2. Schematic representation for synthesis mechanism (a) of mesoporous TiO_2 particles with surfactant and the complex structures (b) of hydrolyzed TTIP-PVP, TTIP-TX and TTIP-P123.

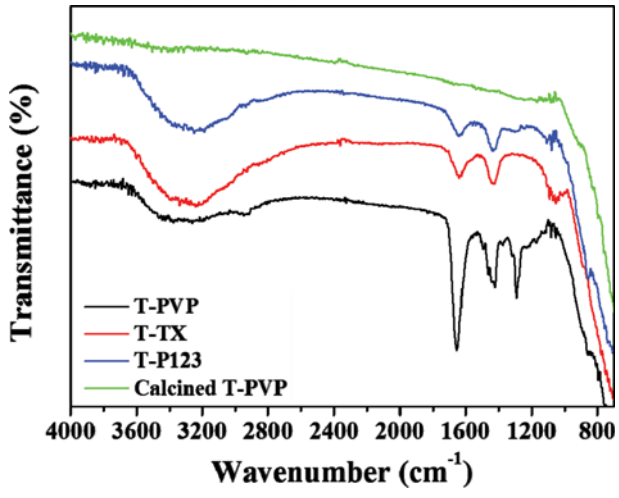

Fig. 3. FT-IR spectra of prepared TiO_2 particles.

coordinated with the titanium cation. The distorted structure could not be restored completely when PVP was removed. These were the reasons why the crystallization of T-PVP differed from that of other TiO_2 [28]. Also, both anatase and rutile phase were observed in the XRD pattern of P25.

N_2 adsorption-desorption isotherm of prepared samples is indicated in Fig. 5. The isotherm pattern exhibited typical type IV

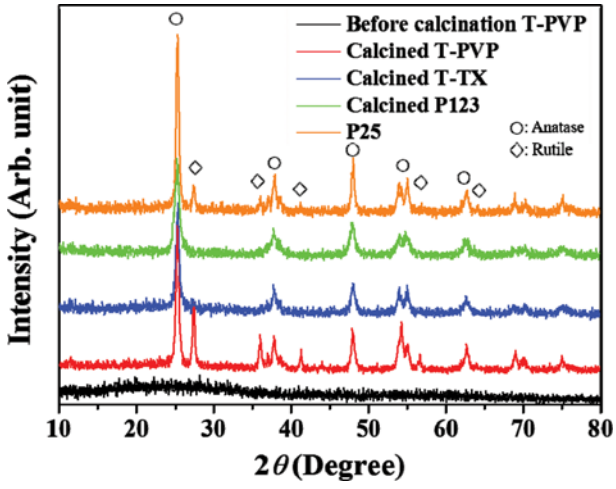

Fig. 4. XRD diffraction patterns of samples.

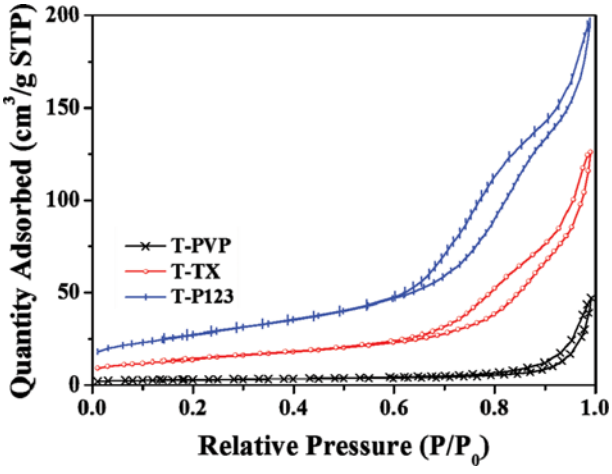

Fig. 5. N_2 adsorption-desorption isotherm curves of samples.

with a hysteresis loop, indicating the characteristics of mesoporous materials based on the IUPAC classification [29]. Their values of BET surface area (S_{BET}), pore volume and average pore diameter of samples are indicated in Table 1. The highest S_{BET} and pore volume were presented in T-P123. It was due to the difference in structure of surfactant. Also, the porosity was increased more as the structure of surfactant was more complex. When eliminating the template, the pores of the mesoporous structures opened up and they became active sites to adsorb the reactant molecules.

3. Photocatalytic Activity

To estimate the photocatalytic activity of prepared TiO_2 powders, the photocatalytic performance for the degradation of MB by TiO_2 was examined under room light irradiation. The photodegradation process of MB could be considered as a Langmuir-Hinshelwood first-order kinetics reaction [30]. The catalytic properties of prepared TiO_2 particles for decay of MB were estimated by using the following equation: MB degradation=$[(C_0-C)/C_0]$, where C_0 (mg/L) was the initial concentration of MB and C (mg/L) was the concentration of MB at a given time interval during the reaction. Their results are indicated and lines represented regression fitting

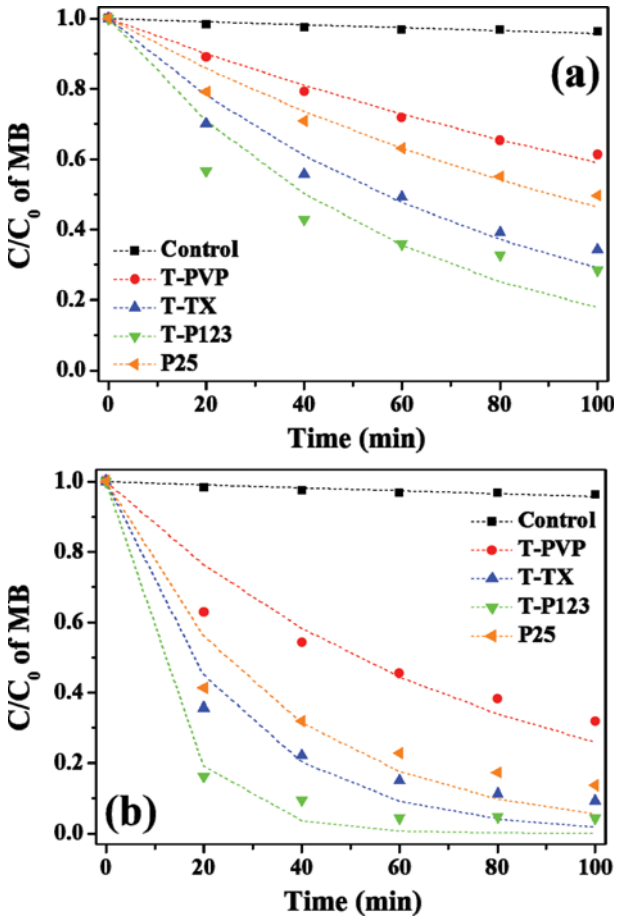

Fig. 6. Photocatalytic activity of samples before (a)/after (b) hydroxylation treatment.

lines in Fig. 6(a) and (b). The correlation constants for the fitted straight line were calculated to be R^2=0.99-0.96. The first-order rate constant could be calculated by using following equation, $kt=-\ln(C/C_0)$, where k and t are first-order rate constant and reaction time, respectively. The values of k are indicated in Table 2. The k value is an important figure, indicating the photocatalytic performance, and the value is proportional to the photocatalytic activity. Compared to P25 as a reference, prepared TiO_2 with PVP samples showed lower photocatalytic activity. Whereas, in the case of T-TX and T-P123, their photocatalytic performance was higher than that of P25, because the active site of catalyst with MB molecules was relative to the surface area. In spite of small surface area, T-TX presented higher photocatalytic activity than that of P25. The crystal structure was an important factor to affect the band gap, resulting in the determination of catalytic performance. Generally, a homogeneous crystal structure was beneficial to higher performance rather than anatase and rutile mixed phase in field of photocatalyst [31]. Thus, it was expected that the higher photocatalytic activity of T-TX was attributed to the homogeneous crystal phase. The highest photocatalytic performance of T-P123 was attributed to the mesoporous structure caused by complex surfactant template in the synthesis process.

To enhance the photocatalytic performance, hydroxylation treatment was performed. The hydroxyl groups on the TiO_2 surface were beneficial to the improvement of photocatalytic activity. Compared to the sample before hydroxylation (Fig. 6(a)), the photocatalytic activity of hydroxylated samples was improved by 2.5-4.8 times as shown in Fig. 6(b) and Table 2. It could be explained by the following reasons. First, the hydrophilic property of catalyst could be enhanced by introducing hydroxyl group on the TiO_2 surface. This resulted in the improvement of dispersibility and adsorption of MB molecules in aqueous solution. As listed in Table 2, the adsorption amount of MB molecule was increased after hydroxylation treatment. It means that the dispersion stability was enhanced by improving the hydrophilic properties of particles. Secondly, the increase of surface hydroxyl concentration has a beneficial effect on the photogenerated charge separation/transfer because the hydroxyl groups could induce the electron transfer from the TiO_2 surface to electron acceptors [2]. Finally, the high density of surface hydroxyl groups increased the trapping sites for photogenerated electron-holes. The trapping sites not only facilitated the charge separation/transfer but also abated the electron-hole recombination.

CONCLUSIONS

Mesoporous structured TiO_2 nanoparticles were synthesized by using simple microwave-assisted sol-gel method. We focused on the research for the effect of surfactants on the formation of TiO_2 nanoparticles. The particle size and specific surface area were effectively controlled by using different surfactants. The mesoporous structured TiO_2 particles prepared with TritonX-100 and P123 exhibited higher photocatalytic activities compared to that of P25. It was attributed to the large surface area and higher porosity by the effect of surfactant on the formation of TiO_2 particles. Furthermore, hydroxylation treatment was performed to introduce the hydroxyl groups onto the calcined TiO_2 surface. Consequently, photocata-

Table 2. Estimations of MB adsorption amount and photocatalytic reaction rate constant (k)

Samples	MB adsorption amount (%)*		k (10^{-3} min^{-1})	
	Before hydroxylation	After hydroxylation	Before hydroxylation	After hydroxylation
T-PVP	0.24	0.42	5.28	13.51
T-TX	0.56	0.96	12.4	39.9
T-P123	1.25	2.35	17.2	82.8
P25	0.85	1.21	7.68	28.9

*Physically adsorbed MB amount during adsorption/desorption step in dark

lytic performance was successfully improved about 2.5-4.8 times.

ACKNOWLEDGEMENT

This research was supported by Korea Electrotechnology Research Institute (KERI) research program funded by Green Energy Innovative Expert (GENIE) (No. 14-02-N0201-07).

REFERENCES

1. A. L. Linsebigler, G. Lu and J. T. Yates, *J. Chem. Rev.*, **95**, 735 (1995).
2. M. R. Hoffmann, S. T. Martin, W. Choi and D. W. Bahnemann, *J. Chem Rev.*, **95**, 69 (1995).
3. X. Chen and S. S. Mao, *J. Chem Rev.*, **107**, 2891 (2007).
4. A. Fujishima and K. Honda, *Nature*, **238**, 37 (1972).
5. J. H. Werner and H. H. Güttler, *J. Appl. Phys.*, **69**, 1522 (1991).
6. J. Yu, L. Qi and M. Jaroniec, *J. Phys Chem. C*, **114**, 13118 (2010).
7. L. Armelao, D. Barreca, G. Bottaro, A. Gasparotto, C. Maccato, C. Maragno, E. Tondello, U. L. Štangar, M. Bergant and D. Mahne, *Nanotechnology*, **18**, 375709 (2007).
8. I. Jang, K. Song, J.-H. Park, M. Kim, D.-W. Kim and S.-G. Oh, *Mater. Lett.*, **96**, 214 (2013).
9. R. Asahi, T. Morikawa, T. Ohwaki, K. Aoki and Y. Taga, *Science*, **293**, 269 (2001).
10. S. Sakthivel and H. Kisch, *Angew. Chem. Int. Ed.*, **42**, 4908 (2003).
11. W. Zhao, W. Ma, C. Chen, J. Zhao and Z. Shuai, *J. Am. Chem. Soc.*, **126**, 4782 (2004).
12. T. Ohno, T. Mitsui and M. Matsumura, *Chem. Lett.*, **32**, 364 (2003).
13. L. Brus, *Appl. Phys. A*, **53**, 465 (1991).
14. C. Wang, X. Zhang, Y. Zhang, Y. Jia, J. Yang, P. Sun and Y. Liu, *J. Phys. Chem. C*, **115**, 22276 (2011).
15. C. Wang, X. Zhang, Y. Zhang, Y. Jia, B. Yuan, J. Yang, P. Sun and Y. Liu, *Nanoscale*, **4**, 5023 (2012).
16. I. Jang, K. Song and S.-G. Oh, *Chem. Lett.*, **41**, 173 (2012).
17. J. Jiang, G. Oberdörster and P. Biswas, *J. Nanopart. Res.*, **11**, 77 (2009).
18. X. Fu, L. A. Clark, Q. Yang and M. A. Anderson, *Environ. Sci. Technol.*, **30**, 647 (1996).
19. J. Yang, J. Zhang, L. Zhu, S. Chen, Y. Zhang, Y. Tang, Y. Zhu and Y. Li, *J. Hazard. Mater.*, **137**, 952 (2006).
20. G. A. Tompsett, W. C. Conner and K. S. Yngvesson, *ChemPhysChem*, **7**, 296 (2006).
21. Y. Wang, Z.-H. Jiang and F.-J. Yang, *Mater. Sci. Eng. B*, **128**, 229 (2006).
22. C. Suwanchawalit and S. Wongnawa, *J. Nanopart. Res.*, **12**, 2895 (2010).
23. K. L. Yeung, S. T. Yau, A. J. Maira, J. M. Coronado, J. Soria and P. L. Yue, *J. Catal.*, **219**, 107 (2003).
24. D. Huang, S. Liao, S. Quan, L. Liu, Z. He, J. Wan and W. Zhou, *J. Mater. Res.*, **22**, 2389 (2007).
25. Y. Zhang and J. Lu, *Cryst. Growth Des.*, **8**, 2101 (2008).
26. S. Doeuff, M. Henry, C. Sanchez and J. Livage, *J. Non-Cryst. Solids.*, **89**, 206 (1987).
27. J. Wu, H. Yan, X. Zhang, L. Wei, X. Liu and B. Xu, *J. Colloid Interface Sci.*, **324**, 167 (2008).
28. M.-P. Zheng, Y.-P. Jin, G.-L. Jin and M.-Y. Gu, *J. Mater. Sci. Lett.*, **19**, 433 (2000).
29. D. H. Everett and L. Haul, *Pure Appl. Chem.*, **57**, 603 (1985).
30. G. W. Roberts and C. N. Satterfield, *Ind. Eng. Chem. Fundam.*, **4**, 288 (1965).
31. J.-H. Park, I. Jang, K. Song and S.-G. Oh, *J. Phys. Chem. Solids*, **74**, 1056 (2013).